Materials Advances

ROYAL SOCIETY OF CHEMISTRY

PAPER

View Article Online
View Journal

Cite this: DOI: 10.1039/d6ma00380j

Surface effects on the magnetic structure and magnetocrystalline anisotropy of $IrMn_3$ from first principles

Robert A. Lawrence [ab] and Matt I. J. Probert *[a]

Received 17th March 2026,
Accepted 5th May 2026

DOI: 10.1039/d6ma00380j

rsc.li/materials-advances

$IrMn_3$ is a key antiferromagnetic material for spintronic devices due to its very high magnetic anisotropy energy. Calculating this requires knowledge of magnetic ordering, which is experimentally challenging to resolve. We use first-principles density functional theory calculations with a novel spin initialisation method to investigate both the magnetic structure and magnetocrystalline anisotropy of $IrMn_3$ surfaces and $IrMn_3$/Fe interfaces. Our new method is based on the epikernel principle using point groups of atomic sites to determine an optimal initial spin configuration. Using this, we find that the Fe on Ir–Mn-[100] has two values of magnetic anisotropy energy depending on the choice of surface termination, and that the perpendicular magnetic anisotropy induced by the Ir–Mn-[111] surface is due to a mechanism that leads to relaxation of the magnetic frustration of the surface layer. These findings highlight the importance of atomic-scale details when designing spintronic devices.

1 Introduction

Magnetocrystalline anisotropy is a key property of materials that are of use within the burgeoning field of spintronics.[1] This intrinsic property, along with domain volume, controls the energy barrier for spin flipping of a domain. There is no universally optimal anisotropy, with many different applications requiring different values for best performance. Soft magnetic materials – those with a low barrier to reversal – are key for applications such as low-loss power transformers whereas hard magnetic materials – with a large barrier – are critical for applications such as data storage, as well as more sophisticated spintronic devices such as magnetic tunnel junctions.[2] For these junctions, biasing the orientation of a ferromagnetic layer using a hard antiferromagnet is key to their function, using a phenomenon known as the exchange bias effect.[3]

The most industrially important antiferromagnet is currently Ir–Mn.[4] While it is widely used due to its high performance, the cost of Ir is prohibitive for large-scale applications; the inelasticity of Ir supply[5] means that any increase in demand will cause a significant rise in cost. To address this, future technologies must either replace Ir–Mn with new high-performance alternatives or maximise its effectiveness so that only minimal amounts are needed. In both cases, a deeper theoretical understanding of the factors driving the high anisotropy of Ir–Mn in spintronic devices will be essential.

The importance of Ir–Mn for spintronic device manufacture[6] has led to extensive experimental and theoretical studies.[7–10] However, there is a scarcity of first-principles theoretical work focusing on the most critical aspect of any device: the interface between layers in the heterostructure. It is at these interfaces that coupling occurs, and deviations from bulk-like properties are not only possible but almost certain. Therefore, gaining greater knowledge and control over these interfaces is crucial for successful device engineering.

Engineers designing devices face many choices – not only which materials to combine at a given interface to achieve desirable electronic (including magnetic) properties, but also which cleavage planes to select for each material. The choice of cleavage plane can significantly affect the final performance of the heterostructure, as different combinations lead to surface states with distinct properties,[11] including variations in magnetic ordering (texture) at the surface and the effective magnetocrystalline anisotropy that determines the exchange bias. In this paper, we explore how interfaces affect the magnetic structure of Ir–Mn thin film layers and how this, in turn, influences the exchange bias[12] that Ir–Mn can induce in a neighbouring soft ferromagnetic layer.[11,13,14]

To better understand the underlying physics governing these interfacial phenomena, it is also instructive to examine the magnetic ordering in two limiting cases: the bulk phase (an interface with itself) and a simple surface exposed to vacuum (an interface with an empty environment). These represent

[a] School of Physics, Engineering and Technology, University of York, York, YO10 5DD, UK. E-mail: matt.probert@york.ac.uk
[b] Department of Physics, University of Tampere, Sähkötalo, Korkeakoulunkatu 3, 33720 Tampere, Finland

the extreme limits of interfaces within a heterostructure: the bulk corresponds to no change at the interface, while the vacuum represents maximal change. Therefore, in addition to studying a heterostructure interface, we also consider the magnetic ordering in both the surface and bulk cases.

Determining the magnetic ordering in an antiferromagnet at an interface is experimentally challenging; device-sized layers are often too thin to be effectively resolved using neutron diffraction or X-ray based techniques, and the presence of electronic surface states means that bulk magnetic ordering may not be preserved. Consequently, computational insights from first-principles simulations are essential for gaining a deeper understanding of magnetic ordering at interfaces. In this work, density functional theory (DFT) is used to perform electronic structure calculations and determine the magnetic order without relying on empirically derived parameters for the bulk material.

A major challenge in modelling magnetic thin films using DFT is that the spin structure creates a multi-minimum problem for the self-consistent field (SCF) procedure (usually implemented using local minimisers), making it possible to converge to a stable solution that may be significantly (up to 10 eV or more) higher in energy than the true magnetic ground state. This issue is typically addressed by ''spin initialisation'', where additional information about the magnetic ordering – often derived from experiment – is used to guide the SCF procedure toward the correct minimum. However, this is not feasible when experimental data are unavailable, such as in the ultra-thin film limit. To address this, we have developed a new method based on the principle of minimal symmetry breaking for spin initialisation. Our symmetry-based ansatz predicts suitable initialisations that lead to the correct magnetic ground state after SCF convergence. This approach does not affect the self-consistency of the final solution and does not require prior knowledge of the exact magnetic ground state – only a sufficiently accurate approximation. Thus, it enables the prediction of magnetic structures from first principles using only the crystal structure, which is already a standard input for DFT methods.

We begin by discussing the spin-initialisation ansatz developed for this work (Section 2.1), followed by an examination of the magnetic ordering in ultra-thin films of Ir–Mn (Section 4.1 onwards) and the effects of interfacing with vacuum *versus* a ferromagnetic capping layer. Finally, we consider the magnetocrystalline anisotropy energy (MAE) of the system as the magnetic orientation of the ferromagnetic capping layer is rotated. For the heterostructure MAE calculations, we selected Fe – a very soft ferromagnetic material – as the capping layer to minimise internal effects from rotating its magnetisation. This combination has also been of experimental interest[14] and serves as a useful proxy for a real device interface.

2 Spin structure initialisation *via* the epikernel principle

One of the major challenges of modelling thin films of $IrMn_3$ with density functional theory is the magnetic ordering. In principle, this is an emergent quantum mechanical property of the system, dependent on the atomic co-ordinates alone. In practice, a multi-minimum potential energy landscape exists for spin configurations, and the local minimisers used during the self-consistent field procedure will optimise towards whichever minimum is closest to the starting configuration.

To counteract this, standard practice is to initialise the initial spins of the unit cell, thereby steering the SCF convergence towards the desired local minimum, which is usually the ground state magnetic structure. This procedure is simple and supported by many DFT codes, but requires *a priori* knowledge of the actual magnetic structure of a system. This is usually not the case for the thin film limit (where the low cross-section of neutron scattering can significantly limit our ability to resolve localised magnetic structure) and especially not true for truly novel structures generated *via* high throughput screening as is becoming commonplace in materials discovery.[15]

In this section we will investigate the use of the ''epikernel principle''[16] and how it may be used to predict magnetic ordering, thereby giving an alternative route to finding an appropriate spin initialisation.

2.1 The epikernel principle

As originally given by Ceulemans *et al.*,[16] the epikernel principle says that the preferred symmetry-breaking direction for a Jahn–Teller unstable crystal is in the direction of a maximal epikernel.[17] An alternative expression is that the extremal points of the PES will correspond to subgroups of the original symmetry which are maximum epikernels, such that both the maximum-energy and minimum-energy symmetry breaking will occur at separate maximal epikernels.

In practice, this means that when the condition for Jahn–Teller distortion is met (degenerate partially occupied bands), the lowest energy state will be reached by a single distortion that preserves as many symmetry operations as possible (it corresponds to the addition of only one of the symmetry functions of the irreducible representations of the degenerate manifold of states excluding the totally symmetric representation). Multiple maximal epikernels may exist for any given system, and these correspond to extremal points in the potential energy surface.

We note, however, that the representation theory approach Ceulemans *et al.* use relies only on the point group of the molecule they considered and an operation it is applied to (in their case, the set of atomic displacements). We also note that the introduction of a magnetic moment to a site is also a valid set of operations that lower the symmetry of the system. We observe their use of the term ''Jahn–Teller unstable'' to indicate partially unoccupied degenerate levels. These partially unoccupied degenerate levels may be energetically unstable with respect to spin polarisation as well as spatial polarisation (displacement). Following this, the same underpinning mathematics may be used. To our knowledge, this present work is the first application of the epikernel principle to spin in magnetic systems.

In the absence of spin–orbit coupling (SOC), magnetic polarisation does not affect the spatial component of the electron orbitals and neither can the underlying symmetry of the crystal

affect the magnetisation orientation. In the presence of SOC, however, this is not the case; L and S are no longer good quantum numbers and the magnetic polarisation is coupled to the lattice degrees of freedom giving rise to a magnetic anisotropy, known as the magnetocrystalline anisotropy. Hence as well as a spin-magnitude (as can readily be approximated from Hund's rules), an orientation is also required to correctly initialise the magnetic system.

For localised magnetic moments (*i.e.* not the itinerant magnetism limit), we note that the associated orbitals must also be tightly confined in space and approximately non-dispersive. In the purely localised moment limit, the orbitals themselves are also purely localised and therefore the symmetry of the electric potential that they are in may be determined purely by knowledge of the local point group of that individual atom. We also know the symmetries of the degenerate orbitals under that point group in terms of their representation. This will be a reducible representation and, as with the Jahn–Teller case, we may apply the epikernel principle to predict the symmetry of the magnetic ground state.

We note that the original Jahn–Teller paper[18] does not explicitly make mention of magnetism; they strictly considered closed shell systems (with the effect of spin-polarised systems for vibrational instability being considered in a follow-up paper by Jahn[19]). This may be remedied by introducing the double groups of Bethe,[20] which – in the same manner that space groups are constructed by combining a crystallographic point group and a translation group – are created by combining an existing (space or point) group with the group {**E**,**R**}, where **E** is the identity operation, and **R** is a rotation by 2π, which differs from identity only when dealing with Fermionic cases. This introduces a new set of representations that apply only to the spins. The use of these double groups underpins our expansion of the Jahn–Teller principle to include magnetic systems, which follows trivially after this change.

Now, for an arbitrary set of degenerate levels, we return to the epikernel principle. A perturbation of magnetic moments may be applied such that it aligns with one (and only one) symmetry function of the symmetry representation of the set of degenerate levels. This breaks the symmetry in such a way that the end state is described by a maximum epikernel. If a symmetry function is chosen that leads to a maximal epikernel corresponding to a maximum in energy, noise within the SCF process will drive the system away from this maximum. This movement from a maximum typically exhibits as single-site spin quenching, making it simple to detect by inspection of the resulting solution. At this point a different maximal epikernel configuration should be chosen until a stable one is discovered.

For low symmetry systems, degeneracies that are enforced by symmetry are less likely; for the cases without degeneracies there are consequently no partially unoccupied degeneracies and hence no symmetry breaking (magnetisation or otherwise) may occur. Low symmetry local point groups are therefore indicative that there is less likely to be a magnetic moment at that point in space. In the case where there is a degeneracy which may be lifted by magnetisation, more directions are contained within the totally symmetric representation (Γ_1 in Bethe notation), and magnetisations aligned thusly can never lift a degeneracy originating in symmetry. Therefore, the high-symmetry case has the most configurations to consider.

We note that by convention when dealing with point groups the local $\hat{z}$ direction is defined to be along the highest order rotation axis (*e.g.* a 6-fold rotation axis is higher order than a 4-fold one). This is entirely independent of the global $\hat{z}$ direction, which is conventionally chosen to align with the $\vec{c}$ axis of the unit cell – although they may be degenerate directions. The rotation axes are found at the intersection of mirror planes, so aligning the spin along rotation axes tends to preserve multiple symmetry operations at once. With higher order rotation axes, there are frequently parallel lower order rotation axes (for example a four-fold axis may have a parallel two-fold axis), and accordingly a symmetry function that obeys the highest-order rotation axis will preserve the most symmetry operations.

The final important concept to introduce is that spin is not a vector but rather a pseudovector. An arbitrary pseudovector $\vec{s}$ transforms under a transformation matrix R, such that $\vec{s}' = \det(R)R\vec{s}$ – and accordingly behaves the same under both proper and improper rotations (and is not affected by mirror planes or inversions). We note that the character of the "doubled" version of symmetry operation **O**, **RO**, has a character of 0 in the extra representations associated with the double group when **O** is an inversion or reflection – this limits the choice of symmetries to rotations (proper or improper). We also note that in many high symmetry groups, the character of twofold rotation axes also becomes 0, making the higher-order axes a more appropriate choice for our initialisation. This leaves us with the result that we wish to choose the highest order rotation axis whether proper or improper as our local $\hat{z}$ direction. In the case of the point groups of the Mn atoms in $IrMn_3$, this is the 4-fold rotation axis normal to the face of the conventional cell containing the Mn atom in question.

In principle, the point group of an atom in an infinite crystal depends on all of the atoms in said crystal. In practice, however, the principle of near-sightedness[21] states that beyond a certain distance, no change will affect our atom. However, the work by Kohn *et al.*[21] does not provide a ready method to determine this distance. At this point we recall that the SCF will change the spin configuration to optimise towards a local minimum, therefore we only require an approximation to the correct spin-density that is sufficiently good as a spin initialisation. As the effects of the nearest neighbours will dominate the local potential, we therefore elect to only consider nearest-neighbour effects when defining the point group of a given atom. Whilst not strictly accurate, this has proved sufficient to enable our initialisation to converge to the correct spin structure, as we shall now discuss.

3 Methods

Density functional theory was used within the plane-wave code CASTEP[22] to simulate the magnetic structures and total

energies of the systems used in this work. In all cases, the Perdew–Wang formulation[23,24] of the LDA exchange–correlation functional was used with non-collinear spin and a full treatment of spin–orbit coupling. A standard Pulay density mixing algorithm[25] was used for all simulations. Further details for specific calculations are given in the following subsections.

3.1 Spin initialisation tests

In order to test the epikernel principle spin initialisation ansatz, bulk $L1_2$ $IrMn_3$ (Fig. 1) was simulated, with both a conventional "correct" (as reported in previous experimental and theoretical studies) and "epikernel principle-predicted" spin initialisation. The epikernel principle-predicted configuration (see blue arrows in Fig. 2) aligns the spin moments along the highest-order rotation axis (normal to the face of the conventional cell that atom is in). A degree of freedom remains for the global spin configuration, since the spin direction is only determined up to a sign. The fully-aligned (net ferromagnetic) configuration was selected, as this was the highest symmetry configuration. The other choice (1 spin anti-aligned with the other two) was also tested and found to yield a state ~8 eV higher in energy.

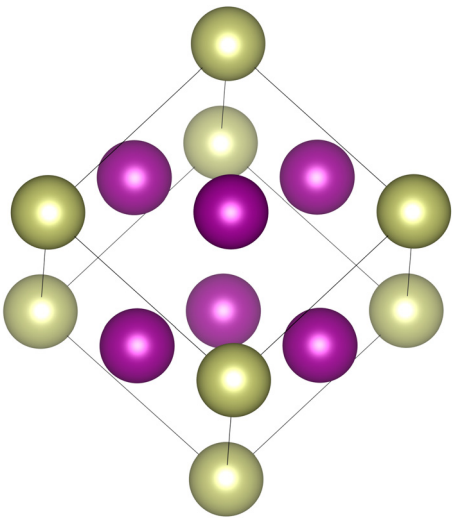

Fig. 1 Bulk structure of $IrMn_3$. The [111] axis is aligned vertically in the page. Gold atoms are Ir and purple atoms are Mn.

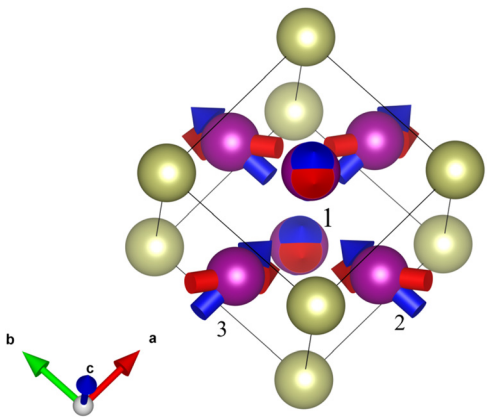

Fig. 2 Bulk $IrMn_3$ including magnetic ordering. Purple atoms are Mn and gold atoms are Ir. Blue arrows represent the ansatz's prediction, and red arrows represent the true spin ground state. Numbers next to the atoms are the label for each atom in Table 1. Note that the ansatz here provides approximately the same structure, saving only a net ferromagnetic moment along the ⟨111⟩ direction.

These were converged using a 2200 eV cut-off energy with the CASTEP NCP-19 library of norm-conserving spin–orbit coupled vector spin pseudopotentials, and a 20 × 20 × 20 Monkhorst–Pack grid was used for reciprocal space sampling of the 4-atom primitive cell. These both converged to the triangular frustrated structure in 20 SCF steps using a Pulay mixing scheme.[25] Other initialisations were attempted, and were found to converge to alternate, higher-energy (metastable) magnetic configurations or not converge. We speculate that the successful convergence from our predicted initial configuration emerged because, whilst technically wrong (it has a net ferromagnetic moment, unlike the real crystal), it yields a magnetic structure in the global minimum potential well of the wider potential energy landscape, whereas other initialisations were closer to local minima, and thereby converged to higher-energy structures under a local minimisation.

3.2 Ultra-thin film $IrMn_3$

For an initial determination of the magnetic structure of the ultra-thin thin films of $IrMn_3$, a 12 × 12 × 1 Monkhorst–Pack grid was used with a 1200 eV cut-off-energy. Since the magnetic ordering has a larger impact on the total energy than spin rotations *via* MAE (eV *vs.* meV), looser SCF convergence parameters can be used to determine the lowest energy magnetic structure. The in-plane lattice parameters were 5.33 Å for the [111] system and 3.77 Å for the [100]-terminated system (see Fig. 3 and 4). This was repeated for the different "epikernel principle-predicted" spin initialisations until the most stable spin configuration for each interface had been found.

These systems then had a bilayer of Fe added on top, such that the underlying crystal structure of the $IrMn_3$ was preserved, in order to mimic the experimental set-up for determining anisotropy in antiferromagnets.[26] This system was not structurally relaxed to ensure that the changes to magnetic ordering were purely down to the change in the interface – from vacuum to Fe.

For the MAE calculations, further detailed in the next subsection, a 2200 eV cut-off energy and a 20 × 20 × 1 k-point grid was used. A vacuum spacing of 10 Å was used throughout, with the spacing being increased on addition of the Fe layer. Finally, the Ir–Mn layers were removed and the difference in MAE for the bulk Fe recorded, which was several orders of magnitude lower in energy ($\mathcal{O}$(μeV)) than the $\mathcal{O}$(meV) MAE for $IrMn_3$.

3.3 Exchange bias calculations of Ir–Mn and Fe heterostructure

Simulating the exchange bias effect directly has the twin advantages of being well-defined (one can deal with the

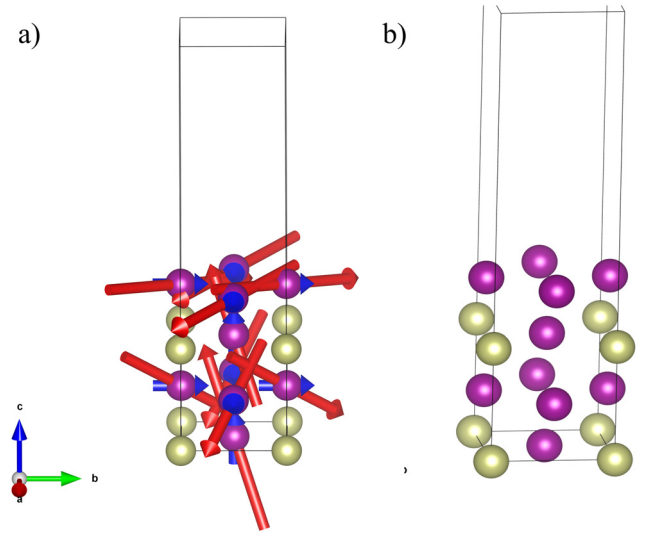

Fig. 3 Panel (a) spin structure of [100] $IrMn_3$ with vacuum. Panel (b) structure of [100] $IrMn_3$ with spins removed for clarity. 3D visualisation for all reported structures may be found in SI. Purple atoms are Mn and gold atoms are Ir. Red arrows represent the spin structure, and blue arrows represent the spin initialisation. Note the different magnetic ordering between the two surface layers; the bottom (Ir and Mn capped) layer is highly resemblant of the bulk magnetic ordering, whereas the top (only Mn capped) layer is highly distorted with a significant in-plane component. This is likely driven by the difference in nearest-neighbour defined environments.

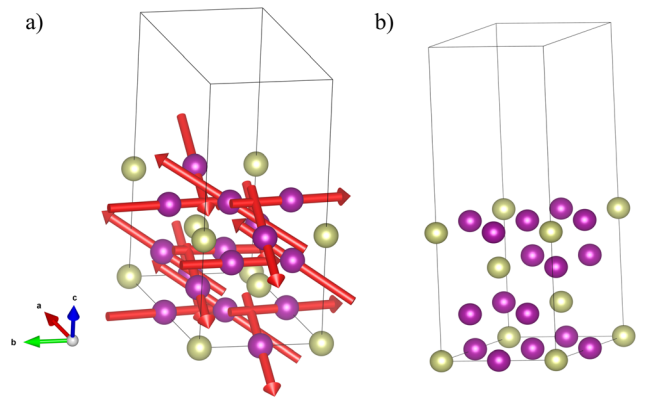

Fig. 4 Panel (a) spin structure of [111] $IrMn_3$ with vacuum. Panel (b) structure of [111] $IrMn_3$ surface with spins removed for clarity. Purple atoms are Mn and gold atoms are Ir. Red arrows represent the spin structure, and blue arrows represent the spin initialisation. Note that the "central" Mn ions that are part of two triangles have a longer magnetic moment.

magnetisation of the FM layer as a single order parameter rather than the multiple Néel vectors of a frustrated antiferromagnet) and being more directly comparable with experimental results since the coupling across the interface is directly included. To simulate this, the outermost layer of Fe in the heterostructure stack had its magnetisation vector rotated through 90 degrees (covering in-plane and out-of-plane orientations) and the energy difference of the system upon rotation was recorded. This was then repeated for the Fe-layer alone to determine the induced anisotropy due to the Ir–Mn.

In order to ensure that the desired magnetic configuration of Fe was sampled, the outermost (furthest from the interface) layer of Fe had its spin orientation constrained,[27] with the rest of the spins in the system free to relax to their lowest energy configuration under that constraint. This ensured sufficient freedom at the interface to ensure that the interfacial interactions were not artificially constrained.

3.4 Visualisation

Ball and stick models and spin-configurations were visualised for all systems using the VESTA software.[28] Suitable VESTA input files have been included in the SI for readers who wish to view a 3-D plot of the spin configurations.

4 Results

4.1 Spin initialisation tests

In order to test the ansatz on a crystal with a known, frustrated antiferromagnetic structure, $IrMn_3$ – which in the bulk phase is known to have a triangular magnetic ordering – was used as a test case. $IrMn_3$ is a cubic alloy of the Cu_3Au ($L1_2$) crystal structure, and belongs to space group 221 ($Pm\bar{3}m$).

This ansatz predicts the directions for the moments should be aligned along the normal of the face of the conventional unit cell in which the Mn atom resides (see Fig. 2). This is in agreement with the reported local easy axis directions by Szunyogh *et al.*[8] The directions of the initial orientation predicted by the ansatz and the true ground state configuration are both reported in fractional co-ordinates in Table 1.

Two separate calculations were run, one with the correct ground state spin structure used as its spin initialisation, and another with the spin structure predicted using the ansatz. All other parameters, including the use of the Pulay mixing scheme, and the energy convergence tolerance of 1×10^{-5} eV per atom were kept the same. These calculations found that the same number (20) of self-consistent field (SCF) cycles were required to attain the ground state for both initialisations, and these final structures were the same within 10 mμ_B magnetisation in any direction.

Table 1 Ansatz-predicted and final state spin structures in fractional co-ordinates (normalised by spin magnitude). The known global ground state structure is conventionally used to initialise the magnetic moments in this cell. In practice, spin magnitudes are initialised with a magnitude of 5μ_B, representing the use of Hund's rules to predict the spin

Mn site	Ansatz initialisation			Ground state structure		
1	0	0	+1	$-\frac{1}{3}$	$-\frac{1}{3}$	$+\frac{2}{3}$
2	0	+1	0	$-\frac{1}{3}$	$+\frac{2}{3}$	$-\frac{1}{3}$
3	+1	0	0	$+\frac{2}{3}$	$-\frac{1}{3}$	$-\frac{1}{3}$

Our ansatz of aligning the local magnetisation with the highest order rotation axis of the local point group within a nearest-neighbour approximation for spin initialisation only seems to be able to reproduce the experimentally confirmed global ground state magnetic structure with a high degree of accuracy for relatively complex frustrated systems. It does not, however, predict global spin-structures (such as FM or AFM structures) which is beyond the capability of a purely localised model.

For the thin-films we will investigate in the second part of this work, such an ansatz is vital – determining the spin structure experimentally is difficult, even assuming that such thin films could be created, and therefore initialising to experimental values is not possible. An exhaustive search of the spin-space, even coarsely, is not practicable due to the exponential scaling of the search space with number of atoms (for example, a 15 degree search mesh in θ–ϕ space would require $288^{N_{\text{atoms}}}$ independent calculations with tightly converged numerical parameters to achieve).

4.2 $IrMn_3$–vacuum interface

Now, we will demonstrate the results of applying the ansatz to determine the spin-configuration of ultra-thin Ir–Mn thin films (reported in SI). Here we use the $IrMn_3$ unit cell as our basis, but induce cleavage planes in the [100] and [111] directions respectively. Within periodic boundary conditions, this enforces the generation of two separate surfaces, thus we are making these simulations in the ultra-thin film limit.

4.2.1 [100] interface. The first thing that may be seen by inspecting the magnetic structure of the [100] cleaved system shown in Fig. 3 is that the magnetic ordering depends on which surface termination is present. Two possible terminations, either Mn-rich or Ir-rich are possible. At the Ir-rich termination, the nearest neighbour interactions for the Mn (the nearest neighbours are the Ir) are indistinguishable from bulk, leading to an approximate preservation of the triangular structure (with some perturbation due to the interfacial effects and breaking of the second-nearest neighbour symmetry). At the Mn-rich interface, however, half of the nearest-neighbour atoms have been removed with the effect that there is a significant rotation of the spins in the Mn-rich surface to being approximately coplanar with the interfacial layer.

With all but the most careful epitaxial growth techniques, a real [100] sample would likely have some combination of the different terminations, as controlling growth to within a fraction of a unit cell is a significant technical challenge. The increased expense associated with controlling this would likely drive the cost too high for commercial applications. Thus a real device constructed using the [100] terminations would have properties that are some weighted average of the two separate surfaces. This average could potentially be influenced by growth conditions (a Mn-rich growth would make Mn-rich termination more likely), or by the effects of any capping layer which will be further investigated in Section 4.3.

4.2.2 [111] interface. A more widely-used interface is the [111] termination.[29] Unlike the [100] case, the constructable terminations are identical, since all [111] planes vary only by a translation. Accordingly, there is only one possible interface that may be obtained from cleaving a bulk crystal along the [111] plane, leading to an increased reliability for device manufacture purposes. This is also reflected in the magnetic structure, where all layers are (barring a translation) nearly the same (the external layers feature slightly larger magnetic moments). It is also worth noting that the [111] cell has a single moment that is shared between two of the triangular motifs, and unlike the bulk case, this atom has a notably larger magnetic moment. This would likely be associated with a stronger coupling to any capping layer's magnetic moments if its presence is robust against the introduction of the capping layer.

4.2.3 Summary of interfaces with vacuum. For both [100] and [111] terminations, the bulk spin structure with its triangular motif is approximately conserved within the core of the layer. At the surfaces, however, the spin structure is highly dependent on the symmetry of the termination. This is indicative of the localised moments being dominated by the nearest-neighbour environment. For the interior layers, the nearest-neighbour defined chemical environment is indistinguishable from bulk, and accordingly the final spin structure ought to be very similar (but not identical, as there are differences due to the thin-film termination disrupting second-nearest neighbour descriptors).

One may consider that the vacuum is in effect a region of high potential with respect to the interior of the crystal, with the difference being the work function. This means that there are large electric fields near the surfaces of the material compared to the interior of the crystal. The $IrMn_x$ family are metallic alloys, and so they have a strong ability to screen electric fields, thereby localising the changes to the surfaces of the crystal. For insulating systems, it is not clear whether the changes to the magnetic structure should be so tightly confined to the surface layer, and further investigations should occur into the effects of surfaces on the magnetic structure of non-metallic systems. Nevertheless, it seems that this observation of vacuum interfaces only strongly-affecting the magnetic ordering at or very near to the surface should be applicable to all metallic systems.

As has been previously noted,[9,10] there has been disagreement within the literature over the spin structure of $IrMn_3$. Some experimental references refer to the spin structure as being collinear,[30] whereas theoretical modelling[8] has determined that bulk $IrMn_3$ has the triangular spin structure reported in Section 4.1. One feature of our results for the spin-structures of thin-film $IrMn_3$ is that the surface-layer has either approximately collinear ordering ($\langle 100\rangle$-termination) or one spin that has a significantly longer moment than the others ($\langle 111\rangle$-termination), both of which could potentially be mistaken for a long-range collinear-ordering when being analysed with experimental methods. Our data also confirm the stability of the triangular magnetic ordering for bulk Ir–Mn for non-surface layers even in the ultra-thin film limit.

4.3 $IrMn_3$–Fe interface

Devices for practical applications typically do not rely on an interface with vacuum. Accordingly, we now turn our consideration

to the effects of capping the previously studied layers with a thin film of Fe. This will give insight into whether real interfaces are more bulk-like or more slab-like in their magnetic ordering, and enable the evaluation of the effect of the termination orientation on induced anisotropy (exchange bias) in a neighbouring soft magnetic material.

4.3.1 [100] interface. The [100] structure created in the previous section contains two distinguishable surfaces – one Ir rich, and one Mn rich. Accordingly, the Fe layer was independently applied to each surface (such that one surface was always interacting with vacuum). The Fe layer was added with the same lattice as the original Ir–Mn thin film. This corresponds to a lattice mismatch of 0.22 Å (~6%) for the [100] surface with [111] Fe and 0.3 Å (~5%) for the [111] surface with 2 unit cells of [100] Fe. These levels of strain can be supported in the ultra-thin film limit. With a thicker Fe layer the system will tend towards a bulk structure and defect formation may occur instead. These structures are presented in Fig. 5 for the Mn-rich surface, and Fig. 6 for the Ir-rich surface.

The largest change induced by the addition of the capping layer is that the quasi-linear spin structure at the Mn-rich surface (see Fig. 3) was restored to a more bulk-like configuration with significant canting of the spins into the layer of the Ir–Mn. This confirms that the symmetry-breaking by removing atoms was the driving force behind the rearrangement, whereas even with a different species of atom present, the bulk-like magnetic ordering continues provided the underlying symmetry of the crystal is unperturbed.

In each figure, two magnetic structures are shown; one with the outermost Fe layer constrained to be in-plane, and one where this layer is constrained to be out-of-plane. All other layers were free to relax. The energetic effects of this are discussed further in Section 4.4.2. We note that for the Ir-rich termination (Fig. 6), the bulk-like magnetic structure of the Fe layer and the non-interfacial layers of the Ir–Mn is conserved and the spin of the sole Mn atom in the Ir-rich interface layer rotates in anti-alignment to the Fe layer in order to minimise the energy. Conversely for the Mn-rich termination (Fig. 5) the spin alignment is approximately constant within the entirety of the Ir–Mn layers, and it is the unconstrained Fe layer that responds. This suggests that a thicker layer of Fe would reduce the associated magnetocrystalline anisotropy, whereas for the Ir-rich termination, the anisotropy would be approximately thickness independent. This very different behaviour dependent only on which termination is capped indicates the importance of atomistic detail for device engineering; it is not only the cleavage plane but also the termination that drives anisotropy. This is in qualitative agreement with ref. 31, who studied the interface between $IrMn_3$ [100]–Fe layer and considered the effect of different layer thicknesses. In this work, we focus instead on the [111] termination, which is of greater technological use as this termination is essential for perpendicular magnetic anisotropy.[32]

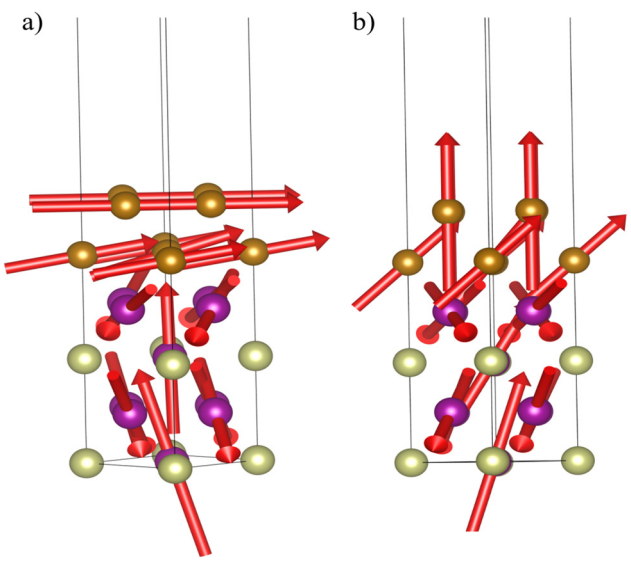

Fig. 5 Magnetic structures for the (a) easy and (b) hard magnetic configurations for Fe on the Mn-rich [100] Ir–Mn surface. Note the easy configuration most closely preserves the magnetic ordering in both the ferromagnetic Fe layer and the antiferromagnetic IrMn layer.

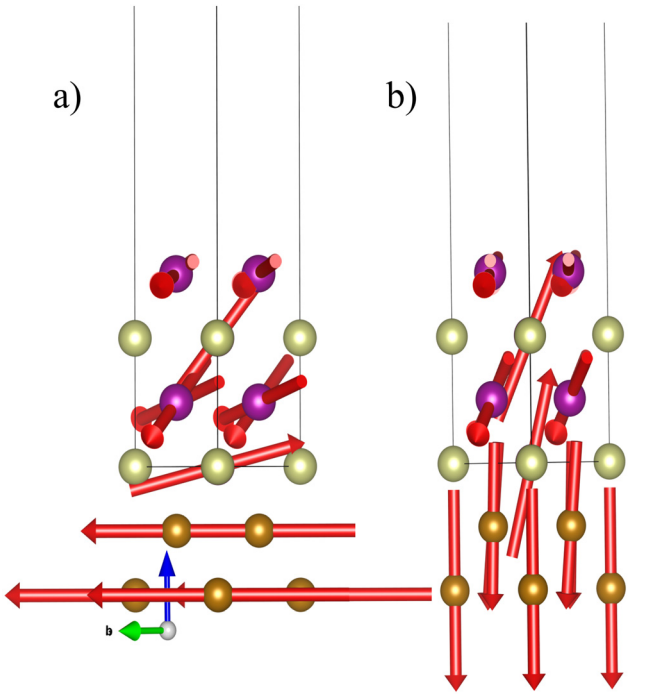

Fig. 6 Magnetic structures for the (a) easy and (b) hard magnetic configurations for Fe on the Ir-rich [100] Ir–Mn surface. The easy configuration has a sharper interface between the two separate magnetic structures with the predominant motion being for the spin on the single Mn at the interface. The deviations are relatively small in the hard-axis case, leading to a reduction in the MAE.

4.3.2 [111] interface. When Fe is added to the [111] surface, there is a distortion of the spin layers in the interface layer only. In the case of perpendicularly aligned magnetic moments, a tetrahedral spin structure forms going across the interface (see panel a of Fig. 7). When the magnetic moments of the Fe are in-plane, the bulk-like magnetic ordering is preserved for the Ir–Mn, and the Fe layer directly on top of the Ir–Mn shows

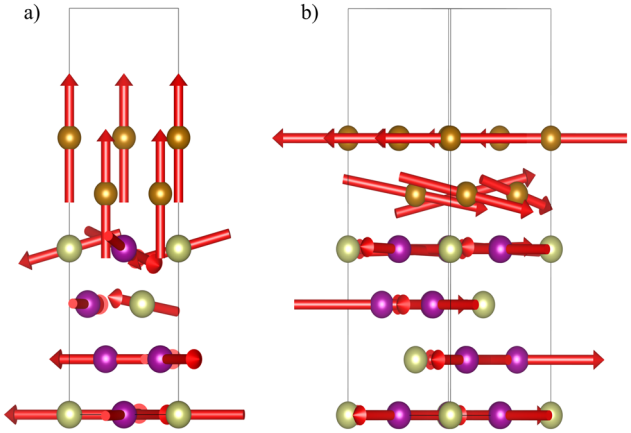

Fig. 7 Magnetic structures for the (a) easy and (b) hard magnetic configurations for Fe on a [111] Ir–Mn surface. 3D visualisation for all reported structures may be found in SI. Note the easy configuration involves a distortion away from the bulk magnetic ordering of Ir–Mn towards the locally easy axes. In panel (a), the apparent spins on the Ir atoms are actually on Mn atoms obscured behind them.

the biggest disruption. This indicates that the perpendicular magnetic anisotropy demonstrated by this system is a direct consequence of the surface state formed when adding the Fe causing more stabilisation than leaving the magnetic order of the IrMn layers unperturbed.

Conversely, the magnetically hard axis is now oriented in-plane (which was the magnetically easy axis for the [100] projection). Additionally, despite an initial ferromagnetic alignment of the two Fe layers, the Ir–Mn has induced an antiferromagnetic ordering between these two layers, leading to an increase in energy compared with the easy axis. It is probable that this is a surface-effect and would decay back to normal ferromagnetic behaviour with increasing depth of Fe added on top of the Ir–Mn layer. It may also indicate that a bilayer of Fe is too small to allow for proper relaxation in this case. Nevertheless, this result – while possibly surprising – strongly suggests the importance of the explicit study of magnetic interfaces when predicting both the magnitude and orientation of the exchange bias effect.

4.3.3 Summary of interfaces with Fe. Since the Fe atoms have been placed on top of the $IrMn_3$ with the same underlying crystal structure (in order to mimic perfect lattice matching), the underlying symmetry of the crystal structure is only weakly perturbed – from the perspective of the Mn atom, the change is much smaller between bulk and interfacing with Fe of matching symmetry than between bulk and vacuum. Accordingly, something closely resembling the bulk magnetic ordering is present in the case of the interface with Fe, whereas clear surface-state associated magnetic orderings may be seen in the case of the vacuum interfaces. Broadly, this implies that with sufficiently high-quality lattice matching the underlying bulk magnetic order will be maintained. We do note, however, that Fe is a transition state metal adjacent to Mn in the periodic table, and as such has very similar chemical properties – so replacing Mn with Fe as a nearest neighbour is a small perturbation. If the interface was with elements that were more dissimilar, such as O (common in magnetic oxides) or B (which forms part of FeCoB – a commonly used capping layer), then this preservation of magnetic order may not persist, especially if there is a poor lattice match, such as with an amorphous seed layer.

It is worth considering the underlying physics driving the choice of easy axis. In both the [100] and [111] cases, the relative energy of the perpendicular and in-plane configurations for the Fe is determined by how ''smoothly'' the transition occurs between the two layers: the smaller the disruption, the lower the total energy. For all of our structures, the surface layer of the Fe is antiferroically aligned with the Mn. For the [111] case, the partial lifting of the frustration reduces the energy, and allows a nearly seamless transition between two quasi-bulk like states.

Whilst we have only simulated the ultra-thin limit, we note that our results are in qualitative agreement with much thicker experimentally-grown samples, where the perpendicular magnetic anisotropy is also found for the [111] surface,[32] but not for [100] growth which favours in-plane anisotropy.[31] This induced anisotropy is not found for thin-film Fe in a vacuum, but rather is emergent as a direct result of the formation of the interfacial surface.

Together, these indicate that the properties of the system with respect to exchange bias are likely to be dominated by the interface effects, with longer range interactions rapidly decaying. This implies that beyond simple lattice matching, ''magnetic order matching'' must also be considered when designing experimental heterostructure systems in order to select for perpendicular magnetic anisotropy (if desired), or to minimise or maximise coupling between the spin moments in the different materials. This is particularly important in cases, such as $IrMn_3$, where the magnetic frustration makes knowledge of both the local and global minimal orientations important.

4.4 Exchange bias of Fe

Magnetocrystalline anisotropy energies (MAE) were calculated for the rotation of the ferromagnetic spin layer of the Fe layers both in the presence and absence of the Ir–Mn layer. The spins were chosen to be either out-of-plane (perpendicular) or in-plane and aligned with the spin-moment of the spin-structure of that plane in the presence of vacuum (parallel). MAE values are calculated as $E_{EB} = E_{perpendicular} - E_{parallel} - \Delta E_{Fe}$ where the ΔE_{Fe} term corrects for the intrinsic anisotropy of the Fe, which is a value on the order of μeV. A negative value of E_{EB} indicates that the in-plane orientation is hard and the system exhibits perpendicular magnetic anisotropy, whereas a positive value indicates that the system prefers the spin to lie in-plane.

4.4.1 Choice of normalisation. Normalisation is an important tool to compare results fairly between different materials. When dealing with bulk-like systems, the two most widely used normalisation factors are per unit volume, and per formula unit. These both correctly capture the extrinsic nature of magnetocrystalline anisotropy, enabling a fair point of comparison. Both, however, have their limitations.

Whilst volume normalisation is easily achieved by using X-ray techniques to determine the size of the sample, it does not account for any possible variation in stoichiometry, or for the fact that surface effects will dominate. In theoretical work, it also is not well-defined in the thin film limit as the thickness of the surface is defined by an exponential decay of electron density into the vacuum region, and therefore the volume is entirely dependent on the choice of threshold for when that has suitably decayed so as to mark the edge of the surface. As a reductio ad absurdum, one could consider that choosing the threshold to be when the electron density associated with this exponential decay reaches precisely 0, then the volume of the thin film would be infinite.

Normalisation per formula unit is more robust with respect to the thin-film thickness problem, and readily comparable between bulk and thin-film theoretical studies, however stoichiometric composition can be hard to determine experimentally, and therefore makes comparison with experiment less direct. This normalisation is also awkward when non-stoichiometric systems are used, such as our [100] surface. To circumvent this difficulty, we choose to normalise by the number of Mn atoms present in the $IrMn_x$ system.

In this paper we will present both area and per Mn normalisations, which avoid the problem of the ill-defined layer thickness and should make comparisons with previously published results sufficiently facile. The ratio of Fe : Mn was constant throughout, so no additional insight is gained from normalising by the number of Fe atoms.

4.4.2 Magnetocrystalline anisotropy energies. The anisotropy of the Fe layers was calculated to be on the μeV scale, and therefore below the lowest significant figure for the magnetocrystalline anisotropy energies (MAE) reported in Table 2. It is worth noting that the [111] surface has a negative MAE – this is due to our calculation of the MAE as $E_{MAE} = E_{out\text{-}of\text{-}plane} - E_{in\text{-}plane}$, so when the in-plane axes are hard (less negative), the sign of the MAE switches to be negative, which solely indicates that the system exhibits so-called ''perpendicular magnetic anisotropy''. This does not suggest a negative barrier for spin-flipping, only the relative orientation of the easy and hard axes.

It is also notable that the exchange bias effect is much weaker for the Ir-rich [100] surface than either of the other two surfaces considered in this study, whereas the Mn-rich surface had a magnitude of anisotropy the same as for the [111] surface. This is indicative that it is the spin–spin coupling between the layers, rather than the biasing of the magnetic moments of the Fe by the presence of Ir, which is critical to the exchange bias effect. This is also an optimistic result for the search to replace Ir with less-scarce alternatives, since it indicates that the high-spin of Mn is more important than the direct presence of Ir to achieve a high magnetic anisotropy.

Finally, we note that there are two competing mechanism driving exchange bias. Firstly, one can have a ''fixed'' AFM layer, where the interfacial layer of the capping material conforms wholly or partially to an unperturbed bulk-like magnetic structure of the AFM. In this case, the increase in energy is almost entirely internal to the FM, and caused by Heisenberg J-couplings and 2-body anisotropies (*i.e.* the misalignment of the spins). By changing the orientation of the capping layer, the degree of misalignment may be minimised, defining the magnetically easy direction. This sort of mechanism was apparent in the Mn-rich [100] termination interface (Fig. 5). This also explains the low anisotropy of the Ir-rich [100] termination, where only a very minimal disruption to the bulk-like magnetic orders emerged, leading to a low MAE.

Alternatively, we also see an additional mechanism for the anisotropy of the [111]-based case. An appropriate magnetic alignment between the two layers can reduce the level of frustration present in the surface layer of Ir–Mn. This reduces the energy of the system. Conversely, an ''unsympathetic'' alignment recovers the previous mechanism, which gives the minimally destabilising rather than an actively stabilising effect. We note that within our ultrathin layers, there is only one layer of magnetic ions within the ferromagnet which are free to rotate. This compresses the distance over which the spins may relax, which could have the effect of increasing the reported anisotropies compared with thicker layers of Fe as thicker layers can support a longer wavelength ''domain wall''. Conversely, we anticipate that the metallic nature of the materials are likely to provide significant screening, such that the distortions to the magnetic ordering converge back to bulk within only a few layers, suggesting that this tight localisation may not be unreasonable. For insulating magnetic materials (not considered in this work) a more thorough investigation of MAE *vs.* capping layer thickness is likely to be critical.

4.4.3 Symmetry breaking at interfaces. It is also worth noting that the maximum amount of achievable exchange bias is not dependent purely on the intrinsic anisotropy of the antiferromagnet. The kinetics of reversal (MAE is the activation energy for this process), are dominated by the minimum energy pathway due to the exponential factor in the Néel–Arrhenius equation. This pathway can leave the antiferromagnet unaffected if disrupting the internal magnetic order of the ferromagnetic capping layer (paying a cost in terms of Heisenberg-J terms) has a lower effective barrier to domain reversal. We may therefore state that the intrinsic anisotropy of the antiferromagnet provides an upper limit to the effective barrier to domain reversal. Accordingly the experimentally measured effective anisotropy depends not just on the intrinsic magnetocrystalline anisotropy of the two magnetic layers, but also on the inter-spin coupling both within and between materials.

Table 2 Magnetic anisotropy values for the three surfaces investigated in this work. Negative values indicate perpendicular magnetic anisotropy (in-plane being a hard plane). Note the [100] surface has a significantly suppressed anisotropy at the Ir-rich surface compared with the Mn-rich layer. Two normalisation schemes are included for convenience, with areal normalisation being given in two separate sets of units (1 meV $Å^{-2}$ = 16.02 erg cm^{-2})

System	erg cm^{-2}	meV $Å^{-2}$	meV per Mn
[100] Ir-rich	2.08	0.13	0.31
[100] Mn-rich	22.3	1.39	3.33
[111]	−26.0	−1.62	−3.33

We have demonstrated that both of these parameters are highly sensitive to the formation of electronic surface states (to say nothing of surface reconstruction).

Further motivation for this can be given by returning to symmetry-based arguments. By adding an interface, we adapt the local symmetries, which can preserve certain symmetry operations (*e.g.* rotations through out-of-plane axes), but break others (*e.g.* in-plane mirror planes). From a quantum mechanical perspective, this can be considered as equivalent to the addition of a ''potential causing deviation from symmetry''. Such a potential is strongest at the interface, and decays rapidly moving away from the interface (giving the observed rapid restoration of bulk-like magnetic order).

This also goes some way to explain the MAE effects: for centrosymmetric systems, neighbouring atoms are in the lowest energy configuration when all spins are aligned (or anti-aligned for antiferromagnetic systems). On breaking of inversion symmetry, locally or globally,[33] a Dzyaloshinskii–Moriya interaction (DMI) term emerges. This term reduces the energy of spin-canting and makes a finite wavelength spin-wave the ground state. This can also stabilise more complicated magnetic structures at boundaries; if deviation from strict alignment is relatively stabilised then the ''domain wall'' between the AFM and FM layers may have a lower energy cost.

4.4.4 Comments on future searches for anisotropic materials. We note that these results clearly indicate the strongly localised behaviour of spin near to interfaces of metallic systems. This is of clear relevance to atomistic spin dynamics, which needs to rely on further DFT simulations (or equivalent quantum methods) to get reliable spatial variations of its key parameters, especially near to interfaces and other defects. These simulations may, in turn, inform device design in commercial contexts.

Finally, we note that these results suggest three promising avenues for further investigation in the search for Ir-free materials for strong exchange bias devices. Firstly, non-collinear antiferromagnetic systems make mechanisms involving removal of frustration for formation of the easy-axis configuration possible, and as such may offer more promising performance than collinear antiferromagnets where this relative stabilisation mechanism is not possible. Secondly, the internal coupling within the already scarce-element-free ferromagnetic layer could be optimised through careful control of composition. This would enable a greater percentage of the intrinsic anisotropy of the AFM layer to affect the biased layer resulting in a device with stronger biasing. Finally, it is clear that symmetry-breaking sites such as interfaces serve as nucleation points or traps for domain reversal, as has been oft-studied in this context for domain wall pinning.[34] Such defects often accumulate near surfaces and interfaces in materials, and so further DFT simulations to inform defect engineering are also desirable.

5 Conclusion

Magnetic structures of thin film $IrMn_3$ systems were studied using a novel method based on spin initialisation determined by the local point group of the atom in question. These predicted a different, lower-energy, spin structure for the surface layer when interfaced with vacuum than in bulk, due to the especially high degree of symmetry breaking in this case. Confinement of the disruption of the bulk-like magnetic ordering to the surface layer may be driven by the metallicity of the system. The precise magnetic structure depended on the surface orientation and choice of termination. When capped with Fe, the bulk-like spin structure was much more noticeable, even at the interface layer. This indicates that the triangular magnetic ordering of the $IrMn_3$ bulk phase is both stable down to very thin (1–2 unit cells thick) films, and that determining the magnetic structure at the interface is highly sensitive to local details; with larger deviations from bulk-like structural order leading to larger changes in the magnetic ordering. Finally, the magnetocrystalline anisotropy energies per unit area were calculated and determined to be 1.39, 0.13, and -1.62 meV Å^{-2} for the [100] Mn-rich, [100] Ir-rich and [111] surfaces.

Conflicts of interest

There are no conflicts to declare.

Data availability

Supplementary information (SI): input files for the CASTEP simulations reported in this paper are available for download from the research data repository of the University of York at DOI: https://doi.org/10.15124/d9c9ef10-036e-4bb5-ab6c-ba8b00207668. VESTA files providing 3-D visualisations of the magnetic structures reported in this work may be found at DOI: https://doi.org/10.15124/1956722d-0813-4adc-96bd-1f59f817064f.

Acknowledgements

The authors acknowledge EPSRC grant EP/V047779/1 for financial support. We are grateful for computational support from the UK national high performance computing service, ARCHER2,[35] for which access was obtained *via* the UKCP consortium and funded by EPSRC grant ref EP/X035891/1.

References

1 M. Misiorny, M. Hell and M. R. Wegewijs, Spintronic magnetic anisotropy, *Nat. Phys.*, 2013, **9**(12), 801–805.
2 K. Samanta, Y.-Y. Jiang, T. R. Paudel, D.-F. Shao and E. Y. Tsymbal, Tunneling magnetoresistance in magnetic tunnel junctions with a single ferromagnetic electrode, *Phys. Rev. B*, 2024, **109**(17), 174407.
3 S. Giri, M. Patra and S. Majumdar, Exchange bias effect in alloys and compounds, *J. Phys.: Condens. Matter*, 2011, **23**(7), 073201.
4 W. Frost, F. Alsaud, R. A. Lawrence, M. Probert and G. Vallejo Fernandez, Towards MnN as a replacement for IrMn, *Sci. Rep.*, 2024, **14**(1), 21944.

5 P. C. K. Vesborg and T. F. Jaramillo, Addressing the terawatt challenge: scalability in the supply of chemical elements for renewable energy, *RSC Adv.*, 2012, **2**(21), 7933.
6 J. Kang, J. Ryu, J.-G. Choi, T. Lee, J. Park, S. Lee, H. Jang, Y. S. Jung, K.-J. Kim and B.-G. Park, Current-induced manipulation of exchange bias in IrMn/NiFe bilayer structures, *Nat. Commun.*, 2021, **12**(1), 6420.
7 A. Carter, S. Jaiswal, P. Campiglio and G. Vallejo-Fernandez, Influence of composition on the magnetisation reversal of IrMn/CoFe exchange bias systems, *J. Magn. Magn. Mater.*, 2024, **598**, 172035.
8 L. Szunyogh, B. Lazarovits, L. Udvardi, J. Jackson and U. Nowak, Giant magnetic anisotropy of the bulk antiferromagnets irmnandirmn$_3$ from first principles, *Phys. Rev. B:Condens. Matter Mater. Phys.*, 2009, **79**(2), 020403.
9 S. Jenkins, R. W. Chantrell, T. J. Klemmer and R. F. L. Evans, Magnetic anisotropy of the noncollinear antiferromagnet IrMn$_3$, *Phys. Rev. B*, 2019, **100**(22), 220405.
10 S. Jenkins, R. W. Chantrell and R. F. L. Evans, Atomistic simulations of the magnetic properties of Ir_xMn_{1-x} alloys, *Phys. Rev. Mater.*, 2021, **5**(3), 034406.
11 N. P. Aley, M. Bowes, R. Kröger and K. O'Grady, Texture and magnetic properties of exchange bias systems, *J. Appl. Phys.*, 2010, **107**(9), 09D722.
12 L. Bufaiçal and E. M. Bittar, Essential aspects of the spontaneous exchange bias effect, *J. Magn. Magn. Mater.*, 2024, **599**, 172109.
13 S. Peng, D. Zhu, W. Li, H. Wu, A. J. Grutter, D. A. Gilbert, J. Lu, D. Xiong, W. Cai, P. Shafer, K. L. Wang and W. Zhao, Exchange bias switching in an antiferromagnet/ferromagnet bilayer driven by spin–orbit torque, *Nat. Electron.*, 2020, **3**(12), 757–764.
14 R. Fan, R. O. M. Aboljadayel, A. Dobrynin, P. Bencok, R. C. C. Ward and P. Steadman, Dependence of exchange bias on structure of antiferromagnet in Fe/IrMn$_3$, *J. Magn. Magn. Mater.*, 2022, **546**, 168678.
15 R. Bhattarai, P. Minch and T. David Rhone, High-throughput screening of altermagnetic materials, *Phys. Rev. Mater.*, 2025, **9**(6), 064403.
16 A. Ceulemans, D. Beyens and L. G. Vanquickenborne, Symmetry aspects of Jahn–Teller activity: structure and reactivity, *J. Am. Chem. Soc.*, 1984, **106**(20), 5824–5837.
17 E. Ascher, Permutation representations, epikernels and phase transitions, *J. Phys. C: Solid State Phys.*, 1977, **10**(9), 1365–1377.
18 H. A. Jahn and E. Teller, Stability of polyatomic molecules in degenerate electronic states - I—Orbital degeneracy, *Proc. R. Soc. London, Ser. A*, 1937, **161**(905), 220–235.
19 H. A. Jahn, Stability of polyatomic molecules in degenerate electronic states ii-spin degeneracy, *Proc. R. Soc. London, Ser. A*, 1938, **164**(916), 117–131.
20 H. Bethe, Termaufspaltung in kristallen, *Ann. Phys.*, 1929, **395**(2), 133–208.
21 E. Prodan and W. Kohn, Nearsightedness of electronic matter, *Proc. Natl. Acad. Sci. U. S. A.*, 2005, **102**(33), 11635–11638.
22 S. J. Clark, M. D. Segall, C. J. Pickard, P. J. Hasnip, M. I. J. Probert, K. Refson and M. C. Payne, First principles methods using CASTEP, *Z. Kristallogr. – Cryst. Mater.*, 2005, **220**(5–6), 567–570.
23 J. P. Perdew and Y. Wang, Accurate and simple analytic representation of the electron-gas correlation energy, *Phys. Rev. B:Condens. Matter Mater. Phys.*, 1992, **45**(23), 13244–13249.
24 J. P. Perdew and Y. Wang, Erratum: Accurate and simple analytic representation of the electron-gas correlation energy [Phys. Rev. B 45, 13244 (1992)], *Phys. Rev. B*, 2018, **98**(7), 079904.
25 P. Pulay, Convergence acceleration of iterative sequences. the case of SCF iteration, *Chem. Phys. Lett.*, 1980, **73**(2), 393–398.
26 K. O'Grady, J. Sinclair, K. Elphick, R. Carpenter, G. Vallejo-Fernandez, M. I. J. Probert and A. Hirohata, Anisotropy in antiferromagnets, *J. Appl. Phys.*, 2020, **128**(4), 040901.
27 P.-W. Ma and S. L. Dudarev, Constrained density functional for noncollinear magnetism, *Phys. Rev. B:Condens. Matter Mater. Phys.*, 2015, **91**(5), 054420.
28 K. Momma and F. Izumi, VESTA3 for three-dimensional visualization of crystal, volumetric and morphology data, *J. Appl. Crystallogr.*, 2011, **44**(6), 1272–1276.
29 A. K. Jana, M. M. Raja, J. A. Chelvane, P. Ghosal and S. N. Jammalamadaka, Ferromagnetic thickness variation exchange bias in IrMn (111)/Fe2CoSi hybrid structure, *J. Supercond. Novel Magn.*, 2022, **35**(5), 1313–1319.
30 K. O'Grady, L. E. Fernandez-Outon and G. Vallejo-Fernandez, A new paradigm for exchange bias in polycrystalline thin films, *J. Magn. Magn. Mater.*, 2010, **322**(8), 883–899.
31 D. Maldonado-Lopez, N. Takeuchi and J. Guerrero-Sanchez, Understanding the noncollinear antiferromagnetic irmn3 surfaces and their exchange-biased heterostructures from first-principles, *ACS Appl. Electron. Mater.*, 2021, **3**(3), 1086–1096.
32 J. Y. Chen, N. Thiyagarajah, H. J. Xu and J. M. D. Coey, Perpendicular exchange bias effect in sputter-deposited cofe/irmn bilayers, *Appl. Phys. Lett.*, 2014, **104**(15), 152405.
33 M. D. S. Dias, S. Brinker, A. Lászlóffy, B. Nyári, S. Blügel, L. Szunyogh and S. Lounis, Proper and improper chiral magnetic interactions, *Phys. Rev. B*, 2021, **103**(14), L140408.
34 V. Zhukova, P. Corte-Leon, L. González-Legarreta, A. Talaat, J. Maria Blanco, M. Ipatov, J. Olivera and A. Zhukov, Review of domain wall dynamics engineering in magnetic microwires, *Nanomaterials*, 2020, **10**(12), 2407.
35 G. Beckett, J. Beech-Brandt, K. Leach, Z. Payne, A. Simpson, L. Smith, A. Turner and A. Whiting, ARCHER2 service description, 2024.